Dalton Transactions

The spectroelectrochemical behavior of redox-active manganese salen complexes

Journal:	*Dalton Transactions*
Manuscript ID	DT-ART-07-2018-002676.R2
Article Type:	Paper
Date Submitted by the Author:	19-Feb-2019
Complete List of Authors:	Solomon, Marcello; The University of Sydney, Chemistry Chan, Bun; Nagasaki University, Graduate School of Engineering Kubiak, Clifford; University of California, San Diego, Department of Chemistry and Biochemistry Jolliffe, Katrina; The University of Sydney, School of Chemistry D'Alessandro, Deanna; The University of Sydney, Chemistry

The spectroelectrochemical behaviour of redox-active manganese salen complexes

Marcello B. Solomon,[a] Bun Chan,[b] Clifford P. Kubiak,[c] Katrina A. Jolliffe,*[a] Deanna M. D'Alessandro*[a]

[a] School of Chemistry, The University of Sydney, New South Wales 2006, Australia, Fax: +61 2 9351 3329; Tel: +61 2 9351 3777; E-mail: deanna.dalessandro@sydney.edu.au; kate.jolliffe@sydney.edu.au

[b] Graduate School of Engineering, Nagasaki University, Bunkyo 1-14, Nagasaki-shi, Nagasaki 852-8521, Japan.

[c] Department of Chemistry and Biochemistry, University of California, San Diego, California 92093, United States

ABSTRACT: Salens are well-known for their ability to catalyse electrochemical transformations; however, despite their rich history, the fundamental reduction chemistry of these systems remains relatively unexplored. This work reports the design and synthesis of eight discrete, functionalised Mn(III) pyridyl salen metal complexes, in which the diamine is varied. The electrochemical properties of the complexes were examined using cyclic voltammetry (CV), spectroelectrochemical (SEC) techniques and Density Functional Theory (DFT) computational modelling to explore the mechanisms that underly Mn salen reduction chemistry. We briefly examine the electrochemistry of these complexes in the presence of CO_2. These complexes represent potential ligands for incorporation into both discrete and extended metallosupramolecular assemblies.

Keywords: Salen complexes, Electroreduction, Electrochemistry, Spectroelectrochemistry

INTRODUCTION

The ubiquity of salen ligands throughout organic and inorganic chemistry over the past eighty years has revealed that they are candidates for many chemical transformations.[1] Since their first reported preparation in 1933 by Pfeiffer,[2] these vibrantly coloured ligand systems have found extensive use in chemical catalysts,[3] electrochemical conversions[4] and charge transfer complexes.[5] The chemical mutability of the salen core leads to the systematic generation of a library of compounds.[6] There is scope to modify the salen backbone to study the steric and electronic influence of substituents (Figure 1). Appending pyridyl groups to the core serves three purposes: to extend the aromaticity of the salen moiety, to endow a greater number of redox processes in the complex,[7] and to anchor redox activity into Metal-Organic Frameworks (MOFs)[8, 9] for use in conductive materials[10-12] and electrocatalysis.[13, 14] Incorporating a bridging diamine in a salen that supports a delocalised π-conjugated system can facilitate improved electrochemical behaviour compared those with aliphatic diamines. In an electrochemical context, the extended π-conjugation has lowered the overpotentials for Co(II) salen-type systems by an additional 0.05 V for the electrosynthesis of 2-phenylacetic acid from CO_2 over their aliphatic components.[4] A recent study by Mazzanti and co-workers has profiled a number of discrete Co(II) salen complexes and their chemically reduced species.[15] The chemical reduction of the complexes by different alkali metals could tune the reduction mechanism of the complex. An important outcome of the work was the elucidation of the chemical reduction mechanism of the Co(II) salen core. The imine radical could reversibly form on the salen core after multiple reductions, resulting in the dimerisation of the complex. The chemically reduced species yielded multiple CO_2 reduction products in the presence of CO_2.

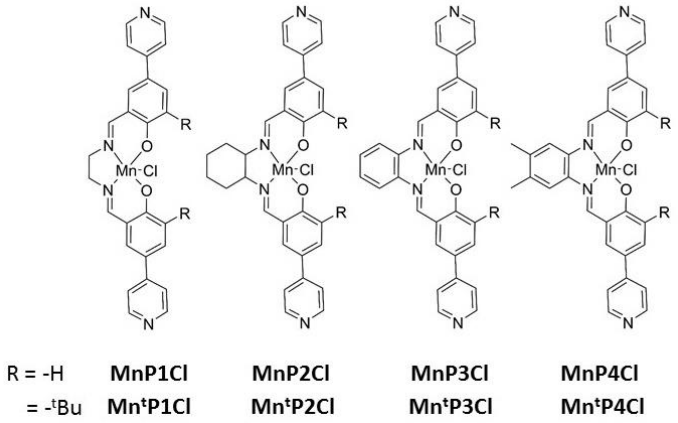

Figure 1. The structures of the eight salen complexes.

Despite the rich literature that exists on the oxidation chemistry of discrete salen metal complexes,[1, 16-23] there are only a few examples of discrete salen metal complexes that have been explored for electrochemical reduction. The impact of electron delocalisation on the electrochemical abilities of the salen core has not yet been studied systematically to the best of our knowledge. The electrochemical reduction of Co(III) containing salen complexes have only been recently been profiled,[24] while Mn(III) complexes, which form the basis of a significant amount of literature for epoxidation reactions[25-34] are yet to be thoroughly investigated.

An important part of electrochemical transformations is the identification of the electrogenerated species. The *in situ* electrogeneration of an active species and its *in situ* spectroscopic characterisation can yield important dynamic data about the active species. The combination of reaction-focused electrochemistry with species-focused spectroscopy has led to the development of spectroelectrochemistry (SEC), which is a powerful tool for the *in situ* analysis of any intermediate electrochemical species. The advantage of SEC is that the changes can be monitored *in situ*, without the need to isolate the active species for its characterisation. The potential is applied directly to the cell, and real-time changes are observed, including the formation of those species that are highly reactive or have a short life span. SEC has been used extensively for probing electrocatalytic mechanisms. The application of IR-SEC to the analysis of CO_2 reduction can be traced back to Chandrasekaran *et al.* in 1987, where an IR band at 1680 cm^{-1} was observed during the direct reduction of CO_2 in acetonitrile. The peak was subsequently studied as a function of potential by Pons and co-workers.[35] Since then, IR-SEC has been used extensively to study the electrocatalysis of CO_2 by transition metal complexes that have diagnostic $\nu_{C=O}$, $\nu_{C=N}$ and $\nu_{pyrazine}$ stretches. SEC methods have been applied readily to the study of [M(bipy)$(CO)_3$Cl] (M = Mn, Re, bipy = 2,2'-bipyridine) complexes.[36] The diagnostic M-CO stretches intrinsic to these metal complexes exhibit strong signals in the IR between 1800–2100 cm^{-1}, which makes them relatively straightforward to track upon the application of electrical potential. UV-Vis-NIR SEC has been used to complement IR SEC studies on the family of [Re(bipy)$(CO)_3$X] complexes.[37] Information about the changes in these complexes could be combined through both forms of SEC to yield a complete picture of the reaction mechanism.[38]

Herein, we describe the synthesis of eight Mn(III) pyridyl-terminated salen complexes in which the bridging diamine is varied. The electrochemical and spectroelectrochemical properties of these complexes have been analysed to determine the mechanism of electrochemical reduction. We also examine the effect of the pendant group (H or ^{t}Bu) on the electrochemical stability of the salen core (Figure 1). We finally profile the electrochemical behaviour of these complexes in the presence of CO_2.

EXPERIMENTAL METHODS

General. All chemicals used were purchased from Aldrich, Alfa Aesar and Merck, and were used without further purification unless stated otherwise. The *tetrakis*(triphenylphosphine) palladium(0) catalyst [Pd$(PPh_3)_4$] was synthesised from palladium(II) chloride (Precious Metals Online) according to the literature procedure.[39] Solvents were obtained from a PureSolv system or purchased and used without further purification. Detailed synthetic procedures are outlined in the Supporting Information.

Cyclic Voltammetry. Solution state electrochemical measurements were performed using a Bioanalytical Systems BASi Epsilon Electrochemical Analyser at 298 K. A single compartment cell was used, consisting of a glassy carbon working electrode (3.0 mm diameter), a platinum wire auxiliary electrode and an electrolysed Ag/AgCl wire reference electrode separated from the solution by a CoralPor tip. Cyclic voltammograms were performed in the analyte (1 mM complex in 0.1 M [$(n$-$C_4H_9)_4$N]PF_6 in either MeCN or DMF (10 mL)). The solution was first purged with dried N_2, Ar, or CO_2 and Ferrocene (Fc) (1 mM) was used as an internal standard. All potentials are quoted in V *vs.* Fc^0/Fc^+. Uncompensated resistance between the working and the reference electrodes was corrected by using

iR compensation. Scan rate dependence studies were carried out for each complex between 50-1600 mVs^{-1} to ensure the homogeneity of the system (Figure S3, S5, Supporting Information).

Infrared Spectroscopy and Spectroelectrochemistry (IR SEC). FT-IR spectra were obtained using a PerkinElmer UATR 2 infrared spectrometer over the range 400–4000 cm^{-1} with a resolution of 4 cm^{-1}. Samples were mechanically compressed on the surface of a diamond crystal.

IR SEC experiments were performed to observe changes in the signature vibrations of the salen-backbone. The experimental design of the IR-SEC cell has been previously reported by Kubiak *et al*.[40] A Pine Instrument Co. Model AFCBP1 potentiostat controlled the cell potential, and was referenced to Ag/Ag^{+}. Thin-layer bulk electrolysis was measured by reflectance IR off the electrode as a function of potential. All experiments were conducted in 0.1 M $[(n\text{-}C_4H_9)_4N]PF_6$/MeCN/DMF (9:1) with known analyte loadings prepared under an inert atmosphere. FT-IR spectra were recorded on a Thermo Scientific Nicolet 6700, with resolution of 4 cm^{-1}, it was not possible to use pure DMF in the IR SEC experiments, since the strong $\nu_{C=O}$ stretching vibration at 1740 cm^{-1} can overwhelm the comparatively weaker $\nu_{C=N}$ stretch expected from the salen metal complex at ~1600 cm^{-1}.

Ultraviolet-Visible-near infrared Spectroelectrochemistry (UV-Vis-NIR SEC). Solution-state UV-Vis-NIR SEC experiments were performed to examine signature changes in the Mn metal centre and electronic transitions. UV-Vis-NIR SEC over the range 5000–35000 cm^{-1} was performed using a CARY5000 spectrophotometer interfaced to Varian WinUV software. In the case where no spectral features were observed between 5000-15000 cm^{-1}, the spectra are only shown from 15000-35000 cm^{-1}. The absorption spectra of the electrogenerated species were obtained *in situ* by using an Optically Semi-Transparent Thin-Layer Electrosynthetic cell, path length 0.685 mm, mounted in the path of the spectrophotometer. Solutions for the spectroelectrochemical experiment contained 0.1 M $[(n\text{-}C_4H_9)_4N]PF_6$/MeCN or $[(n\text{-}C_4H_9)_4N]PF_6$/DMF supporting electrolyte and *ca.* 0.4 mM of the compound for analysis. Appropriate potentials were applied by using an eDAQ e-corder 410 potentiostat and the current was carefully monitored throughout the electrolysis. The electrogenerated species were obtained *in situ*, and their absorption spectra were recorded at regular intervals through the electrolysis. The attainment of a steady-state spectrum and the decay of the current to a constant minimum at a potential appropriately beyond $E_{½}$ (for the redox process) was indicative of the complete conversion of the starting material.

Computational details. Standard computational chemistry calculations were carried out with Gaussian 16[41] and geometry optimisations were carried out at the B-PW91/6-31G(d) procedure.[41,42] Calculations at the B3-PW91/6-311+G(3df,2p) level[43] were conducted to obtain an improved description of the electron density for subsequent NBO analysis.[44] These methods were chosen based on the consideration of a balanced and reliable treatment for both the organic moieties and the transition-metal centre.[45,46] All calculations were carried out with the inclusion of a solvent continuum using the SMD model[47] and the parameters for DMF to reflect typical experimental conditions. Tabulated relative energies for the various species at different redox states and optimised geometries are provided in the supporting information.

RESULTS AND DISCUSSION

Synthesis

The synthesis of 3-*tert*-butyl-2-hydroxy-5-(4-pyridinyl)-benzaldehyde (**1^t**) was achieved in two steps, involving the electrophilic aromatic substitution of 3-*tert*-butyl-2-hydroxy-benzaldehyde, followed by a Suzuki coupling with 4-pyridyl boronic acid to give the desired product as a light yellow oil in good yield (Scheme S1A, Supporting Information). The synthesis of 2-hydroxy-5-(4-pyridinyl)-benzaldehyde (**1**) was achieved under similar conditions (Scheme S1B, Supporting Information).

The synthesis of the aliphatic and aromatic pyridyl-terminated salen complexes was achieved through the Schiff-base condensation of either **1** or **1^t** with the chosen diamine (Scheme S1C, Supporting Information). The target compounds were obtained in good yields (Figure S1, Supporting Information). Four unique bridging diamines were chosen to underpin the electronic studies of the discrete complexes. The diamines (1,2-ethylenediamine, 1*R*,2*R*-di-aminocyclohexane, *o*-phenylenediamine and 4,5-dimethyl-*o*-phenylenediamine) vary in size, aromaticity and alter the electron delocalisation across the molecule, giving rise to interesting electronic properties.[5, 48, 49]

Salen complexes were metallated by the drop-wise addition of $Mn(OAc)_2 \bullet 4H_2O$ (1.1 eq.) to a vigorously stirred solution of the salen in EtOH under N_2 at room temperature. Following coordination of the Mn(II) centre has coordinated, the reaction was exposed to air to chemically oxidise Mn(II) to Mn(III). The addition of LiCl yielded a Mn(III) complex, with charge balance afforded by a chloride ion. (Scheme S1C, Supporting Information). The syntheses of these Mn(III) metal complexes were achieved in good yields (Figure S1, Supporting Information).

Electrochemistry

Solution state CV experiments were performed on all Mn(III) salen metal complexes (Table 1 and Figure S2, Supporting Information). For the aliphatic salen complexes, mostly irreversible processes were observed after the initial reduction. The increased size of the aliphatic bridging diamine may inhibit charge transfer across the complex, shifting the reduction processes anodically. An aromatic backbone does not significantly alter the reduction processes, while the addition of an electron donating moiety cathodically shifts the redox processes. The salen backbone has a rich electron density, making it difficult for the salen to accept any additional charge after a ligand-based reduction.

Table 1. Redox features for Mn(III) salen metal complexes where R = H. Ferrocene (1 mM) was used as an internal standard. Where available, the peak-peak separation (ΔE) and the current ratio (i_{pa}/i_{pc}) of reversible and *quasi*-reversible redox features have been described. I_R-III_R define the first-third reduction processes, respectively.

Complex	I_R	II_R	III_R
MnP1Cl	–0.69 V[b]	–2.63 V[a]	–2.87 V[b]
MnP2Cl	–0.66 V[a]	–2.44 V[a]	–2.78 V[a]
MnP3Cl	–0.46 V[c]	–2.23 V[a]	–3.01 V[a]
MnP4Cl	–0.56 V[a]	–2.25 V[a]	

[a] irreversible E_{pc} [b]*quasi*-reversible $E_{½}$, ΔE = 76 mV, (i_{pa}/i_{pc}) = 0.877 **Fc:** ΔE = 60 mV, (i_{pa}/i_{pc}) = 0.966 [c] *quasi*-reversible $E_{½}$, ΔE = 74 mV, (i_{pa}/i_{pc}) = 0.583 **Fc:** ΔE = 59 mV, (i_{pa}/i_{pc}) = 0.933

The presence of the *tert*-butyl group on the salen core improves the reversibility of the first observable reduction processes, suggesting that it provides a stabilising effect (Table 2 and Figure S4, Supporting Information). The aliphatic complexes had improved stability compared to their non *tert*-butyl analogues, despite the slight cathodic shift in their processes (expected from the more electron donating nature of the *tert*-butyl moiety). Moving from ethylenediamine (**Mn^{t}P1Cl**) to diaminocyclohexane (**Mn^{t}P2Cl**) led to a cathodic shift in the redox processes and decreased their reversibility, as noted for the non *tert*-butyl analogues. Distinct differences were observed between the CVs of the aromatic and aliphatic salen metal complexes. The first one electron processes of **Mn^{t}P3Cl** and **Mn^{t}P4Cl** were accessible at lower potentials and were more reversible than their aliphatic counterparts. Including an electron donating methyl group to **Mn^{t}P4Cl** cathodically shifted the initial reduction process.

Table 2. Redox features for Mn(III) salen metal complexes where R = *tert*-butyl. Ferrocene (1 mM) was used as an internal standard. Where available, the peak-peak separation (ΔE) and the current ratio (i_{pa}/i_{pc}) of reversible and *quasi*-reversible redox features have been described. I_R-V_R defines the first-fifth reduction processes, respectively.

Complex	I_R	II_R	III_R	IV_R	V_R
Mn^{t}P1Cl	–0.69 V[b]	–2.24 V[a]	–2.59 V[a]	–2.89 V[a]	–3.11 V[a]
Mn^{t}P2Cl	–0.74 V[c]	–2.52 V[a]	–2.80 V[a]	–3.11 V[a]	
Mn^{t}P3Cl	–0.53 V[d]	–2.23 V[e]	–2.60 V[a]		
Mn^{t}P4Cl	–0.55 V[f]	–2.35 V[a]	–2.49 V[a]		

[a] irreversible E_{pc} [b]reversible $E_{½}$, ΔE = 63 mV, (i_{pa}/i_{pc}) = 0.958 **Fc:** ΔE = 61 mV, (i_{pa}/i_{pc}) = 0.977, [c]*quasi*-reversible $E_{½}$, ΔE = 86 mV, (i_{pa}/i_{pc}) = 0.701 **Fc:** ΔE = 59 mV, (i_{pa}/i_{pc}) = 0.988 [d]*quasi*-reversible $E_{½}$, ΔE = 69 mV, (i_{pa}/i_{pc}) = 0.862 **Fc:** ΔE = 67 mV, (i_{pa}/i_{pc}) = 0.941 [e]*quasi*-reversible $E_{½}$, ΔE = 82 mV, (i_{pa}/i_{pc}) = 0.427 **Fc:** ΔE = 67 mV, (i_{pa}/i_{pc}) = 0.941 [f]*quasi*-reversible $E_{½}$, ΔE = 81 mV, (i_{pa}/i_{pc}) = 0.810 **Fc:** ΔE = 59 mV, (i_{pa}/i_{pc}) = 0.957

Evidence for the mechanism of reduction for Mn(III) salen complexes containing an aliphatic bridging diamine (based on Mn^{t}P1Cl)

The CV of **Mn^{t}P1Cl** revealed one *quasi*-reversible process and four irreversible processes. The proposed electrochemical reduction is based on a detailed study of the IR and UV-Vis-NIR SEC obtained from the complex (Scheme 1). Only the first three reduction processes have been examined, as spectroelectrochemical data suggest that subsequent reductions occur on degraded species. DFT computations for the representative **Mn^{t}P1Cl** complex were performed to further validate the proposed mechanism. The SEC data for other salen metal complexes containing aliphatic diamines is discussed in the Supporting Information (Figures S6-S10).

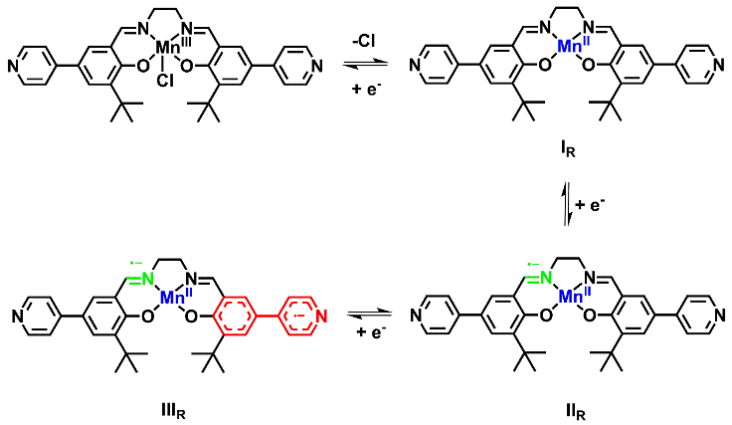

Scheme 1. Proposed mechanism for the reduction of **Mn^{t}P1Cl** in the absence of DMF after one, two and three electron reductions.

The starting spectrum of **Mn^{t}P1Cl** contained bands at 15860, 20610, 23330, 27320, 30810 and 33100 cm^{-1} while the starting IR spectrum contained an imine stretch at $\nu_{C=N}$ = 1597 cm^{-1} . The UV-Vis-NIR spectrum of the Mn(III) salen core without the pyridyl groups has been previously reported by Zidane *et al.*, showing similar bands.[50] For this core, charge transfer bands appeared at 16000, 20410, 25000 and 30770 cm^{-1}, respectively. The I_R redox process of **Mn^{t}P1Cl** at $E_{½}$ = –0.69 V *vs.* Fc^0/Fc^+ (Figure 2) was investigated by UV-Vis-NIR SEC and was ascribed to a Mn(III/II) reduction. New charge transfer bands were observed at 23740 and 28180 cm^{-1}, which were accompanied by a decrease in the band at 33100 cm^{-1}. There were no significant changes observed in the ligand based vibrational frequencies using IR SEC. The present spectra are therefore consistent with an increase in the LMCT and n-π* transitions upon reduction. The presence of clear isosbestic points indicates that there is only one process occurring, with no chemical decomposition, supporting the *quasi*-reversible nature of the process observed in the CV.

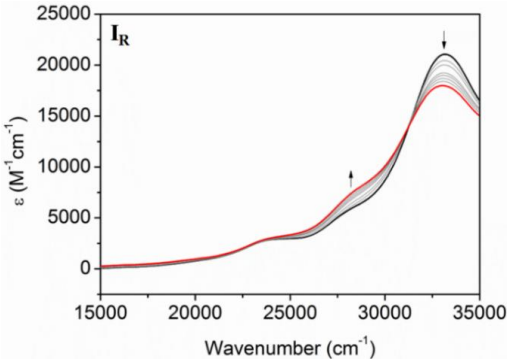

Figure 2. Solution state UV-Vis-NIR SEC of **Mn^{t}P1Cl** (0.38 mM) upon changing the potential from +0.4 to –0.3 V vs. Ag/Ag^+ (0.1 M $[(n\text{-}C_4H_9)_4N]PF_6$/DMF as the supporting electrolyte).

The II_R process of **Mn^{t}P1Cl** was assigned to the reduction of the imine moiety of the salen complex (Figure 3A, 4C). Upon the application of a potential at E_{pc} = –2.59 V *vs.* Fc^0/Fc^+, the IR SEC revealed a shift of the imine peak

to lower energies, consistent with a ligand-based redox process.[51] The change in the IR spectrum upon reduction was accompanied by significant changes in the UV-Vis-NIR spectra, where the growth of bands at 23740 and 28180 cm^{-1} indicate a change in the electronic interactions across the complex associated with the LMCT and n-π* transitions. The maintenance of the isosbestic points indicates that there is only one transformation occurring.

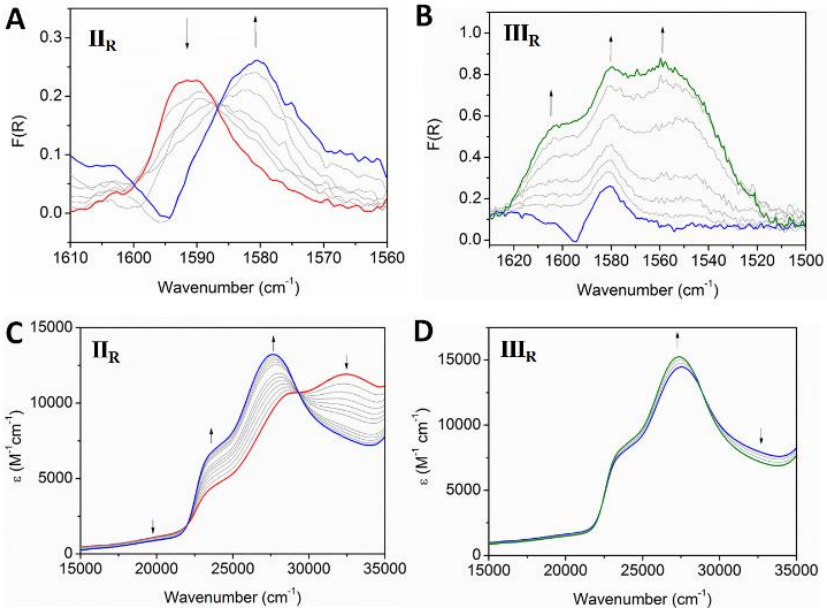

Figure 3. Solution state IR SEC of **Mn^{t}P1Cl** (4mM) upon increasing the potential from **A** −1.1 to −1.7 V *vs*. Ag/Ag^+ and **B** −1.8 to −2.4 V *vs*. Ag/Ag^+. Solution state UV-Vis-NIR SEC of **Mn^{t}P1Cl** (0.38 mM) upon increasing the potential from **C** −1.1 to −1.7 V *vs*. Ag/Ag^+ and **D** −1.8 to −2.4 V *vs*. Ag/Ag^+. IR SEC was measured in 0.1 M [(*n*-$C_4H_9)_4N]PF_6$/MeCN/DMF (9:1) as the supporting electrolyte, while UV-Vis-NIR SEC was measured in 0.1 M [(*n*-$C_4H_9)_4N]PF_6$/DMF as the supporting electrolyte.

The III_R redox process for **Mn^{t}P1Cl** at E_{pc} = −2.89 V *vs*. Fc^0/Fc^+ corresponds to a ligand-based process (Figure 3B and 4D). In the IR SEC, two broader bands appearing at 1610 and 1555 cm^{-1} are tentatively assigned to processes from the phenoxy ring[52] and the pyridyl ring,[53] respectively, and are consistent with a radical anion forming on the salen. The preservation of the radical $\nu_{C=N}$ band indicates that the dianionic system is asymmetric and is likely to have a radical on either side of the core. The irreversibility of both processes indicates that the singly and doubly reduced species may dimerise, and is further supported by the inability to retrieve the starting spectrum. Minor changes in the charge transfer bands from the UV-Vis-NIR SEC data implies that the second radical may not be near the Mn(II) centre. The unstable product from the III_R process was reflected in the complexity of the CV at higher cathodic potentials, so further processes were therefore not examined spectroscopically.

Computational Evidence for the reduction of Mn^{t}P1Cl

DFT calculations on the model systems (Table S1, Supporting Information) indicate that **Mn^{t}P1Cl** is likely to exist in DMF solution as a quintet complex with relatively labile Cl^- and DMF ligands. The complete dissociation of the system is still energetically unfavourable, costing approximately 40 kJ mol^{-1}. Comparatively, the singly reduced species results in an almost thermoneutral dissociation of the two ligands from the resulting quartet complex. Calculations on model systems suggest that further reductions increasingly favour dissociation of the two ligands, but more importantly lower their spin states. These observations on the model systems are kept in mind when computing the full species. Therefore, the focus is on the complexes excluding the Cl^- and DMF ligands, i.e., **Mn^{t}P1**. An analysis of the spin distribution within the quintet [**Mn^{t}P1**]$^{+1}$ state reveals essentially four unpaired electrons at the Mn centre (Figure 4), with an NBO α-spin of 3.83, and some small spins distributed to nearby atoms. In comparison, for the singly reduced quartet [**Mn^{t}P1**]^{0}, the α-spin at the Mn atom is 3.14. This is consistent with a metal-centred reduction process for I_R, with the additional (β) electron essentially paired with an α-electron on Mn. It is observed that the additional electron also has a spill-over effect of causing small spin polarisation in nearby atoms and at the Mn centre itself (such that the spin is still in excess of 3).

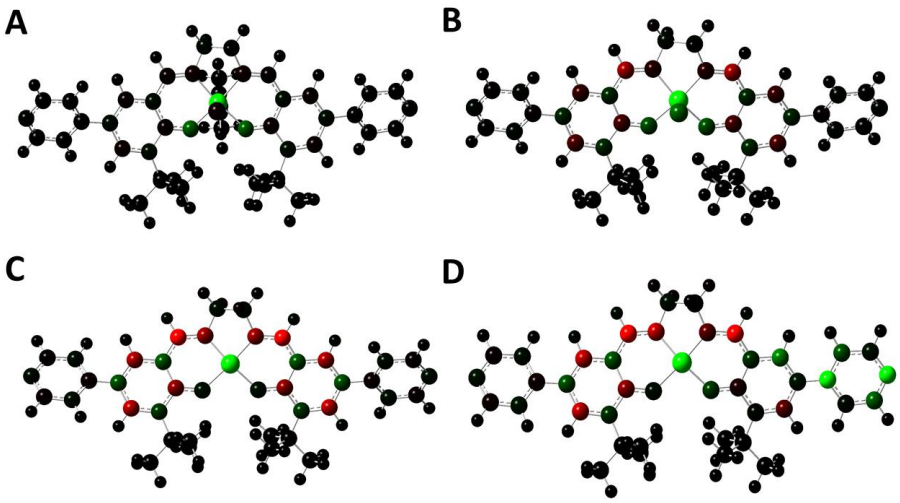

Figure 4. Colour representation of spin distribution with a range of –0.25 to +0.25 in **A** [**Mn^{t}P1**]^{0}, **B** [**Mn^{t}P1Cl**]$^{-1}$, **C** [**Mn^{t}P1**]$^{-1}$, and **D** [**Mn^{t}P1**]$^{-2}$. Green represents excessive α-spins (up to 5), red represents (to different magnitudes) β-spins (up to –0.5), and black represents close to neutral states.

Analysis on the NBO spin density of the doubly reduced species (i.e. II_R – [**Mn^{t}P1**]$^{-1}$) shows that the Mn atom maintains a net α-spin of 3.36, which implies that the additional (β) electron from II_R is absorbed mostly by the ligand in a delocalised manner, which can be seen visually (Figure 4C). Detailed inspection of the spin distribution pattern indeed shows an even distribution between the two sides of the ligand. As the two parts are "supposedly insulated" from one another with the alkyl linkage, the delocalised nature of the radical anionic ligand suggests a through-metal communication mechanism.

Computational studies with model compounds after three reduction processes (i.e. III_R – [**Mn^{t}P1**]$^{-2}$) suggest that [**Mn^{t}P1**]$^{-2}$ has two low-lying spin states (doublet and quartet) that are close in energy. For the doublet, the Mn

centre has a net NBO α-spin of 2.65, implying that the additional β electron is mostly ligand based. Likewise, for the quartet (Figure 4D), the additional electron in going from [**Mn^{t}P1**]$^{-1}$ to [**Mn^{t}P1**]$^{-2}$ can be seen in the ligand. In this case, the excess α-spin in [**Mn^{t}P1**]$^{-2}$ at the Mn is 3.29. The nature of the [**Mn^{t}P1**]$^{-2}$ species is fully consistent with the experimental observations. It can also be seen that the additional α-spin on one pyridine causes, as one would anticipate, certain subtle spin polarisation, such that the excess β-spin that was originally distributed evenly between the two sides in [**Mn^{t}P1**]$^{-1}$ is now somewhat concentrated on one side of the ligand.

Evidence for the mechanism of reduction for Mn(III) salen complexes containing an aliphatic bridging diamine (based on Mn^{t}P3Cl)

The CV of **Mn^{t}P3Cl** revealed two *quasi*-reversible processes and one irreversible process. Evidence for the proposed electrochemical reduction was elucidated from the IR and UV-Vis-NIR SEC data (Scheme 2). DFT computations for **Mn^{t}P3Cl** were performed to validate the proposed mechanism. A comparison to the SEC data for other aliphatic salen metal complexes is provided in the supporting information (Figure S11-S14, Supporting Information)

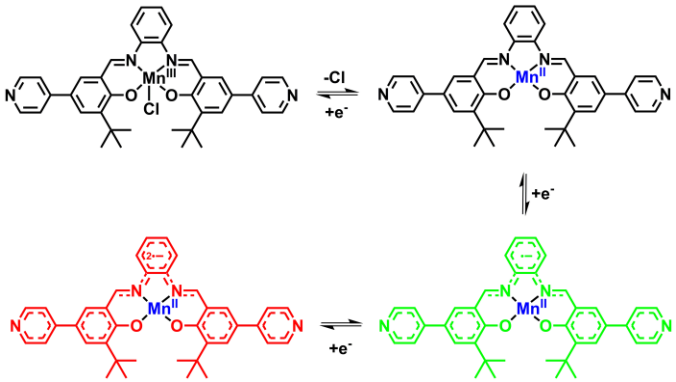

Scheme 2. Proposed mechanism for the reduction of **Mn^{t}P3Cl** in the absence of DMF after one, two and three electron reductions.

Literature reports for the UV-Vis-NIR spectrum of the neutral aromatic Mn(III) salen core show a *d-d* band at 21280 cm^{-1} and n-π* transition at 27620 cm^{-1}.[54] In the solution state UV-Vis-NIR SEC experiments, I_R at $E_{½}$ = –0.53 V *vs.* Fc^{0}/Fc^{+} was characterised by the appearance of bands at 21880, 23930 and 29330 cm^{-1}, while the bands at 20540, 27320 and 32910 cm^{-1} disappeared (Figure 5). The loss of the weak *d-d* band at 20540 cm^{-1} is consistent with the change from high spin Mn(III) to Mn(II) (d^4 to d^5) transition, supporting the assignment as a Mn(III/II) reduction process.

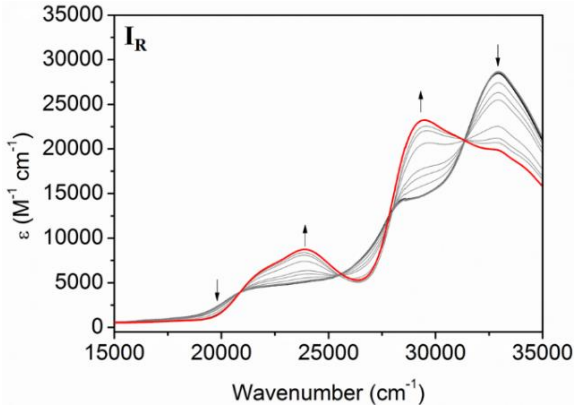

Figure 5. Solution state UV-Vis-NIR SEC for process I_R of **Mn^{t}P3Cl** (0.36 mM) upon changing the potential from 0.4 V to −0.1 V *vs.* Ag/Ag^+ (0.1 M $[(n\text{-}C_4H_9)_4N]PF_6$/DMF as the supporting electrolyte).

The II_R process in the CV of **Mn^{t}P3Cl** at E_{pc} = −2.32 V *vs.* Fc^0/Fc^+ was analysed by IR and UV-Vis-NIR SEC (Figure 6). The $\nu_{C=N}$ stretch at 1594 cm^{-1} in the IR disappeared completely upon the application of the potential, while the charge transfer bands at 22500 cm^{-1} and 27000 cm^{-1} in the UV-Vis-NIR increased. This differs slightly to the observations made for **Mn^{t}P1Cl**, which are consistent with the aromatic nature of the backbone facilitating delocalisation of charge across the bridging diamine and imines. The presence of isosbestic points indicates that only one species is appearing upon electrochemical reduction. There was a significant difference between the spectral responses for the bands associated with II_R for the aromatic **Mn^{t}P3Cl** and aliphatic **Mn^{t}P1Cl** complexes. The incorporation of the aromatic bridging moiety facilitates delocalisation of the radical formed upon reduction across the backbone of the salen, and is consistent with the disappearance of the $\nu_{C=N}$ stretch in the aromatic systems.

The III_R redox process at E_{pc} = −2.60 V *vs*. Fc^0/Fc^+ in the CV of **Mn^{t}P3Cl** is tentatively ascribed to the generation of a salen-based radical anion. The IR SEC experiment reveals the appearance of a broad band at 1550 cm^{-1}, consistent with literature reports for a pyridyl-type radical anion.[53] Further evidence for this is provided by the UV-Vis-NIR SEC experiments, where moderate changes in the charge transfer bands were observed and somewhat more noticeable changes appear in the π-π* region.

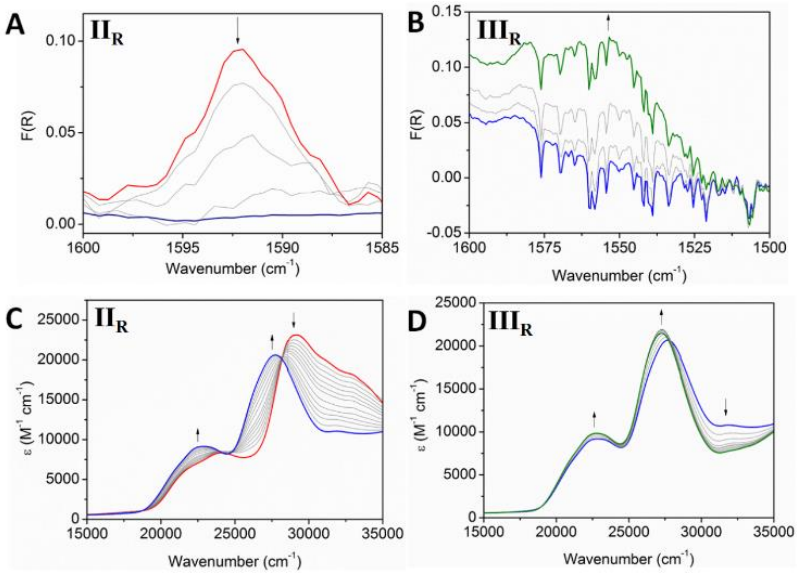

Figure 6. A Solution state IR SEC of **Mn^{t}P3Cl** (4 mM) upon increasing the potential from –1.3 to –1.7 V *vs.* Ag/Ag$^+$ and **B** –1.8 to –2.1 V *vs.* Ag/Ag$^+$. **C** Solution state UV-Vis-NIR SEC of **Mn^{t}P3Cl** (0.36 mM) upon increasing the potential from –1.3 to –1.7 V *vs.* Ag/Ag$^+$ and **D** –1.8 to –2.4 V *vs.* Ag/Ag$^+$. The supporting electrolytes were 0.1 M [(*n*-C$_4$H$_9$)$_4$N]PF$_6$/MeCN/DMF (9:1) for IR SEC or 0.1 M [(*n*-C$_4$H$_9$)$_4$N]PF$_6$/DMF for UV-Vis-NIR SEC.

Computational Evidence for the reduction of Mn^{t}P3Cl

DFT calculations for **Mn^{t}P3Cl** suggest that the I_R process for [**Mn^{t}P3**]$^{+1}$ is a metal-centred process akin to that observed for the aliphatic [**Mn^{t}P1**]$^{+1}$, but they also reveal differences stemming from the aromatic linker (Figure 7). The excess α-spin at the Mn centre within quintet [**Mn^{t}P3**]$^{+1}$ is 3.84, which is almost identical to the corresponding value of 3.83 in [**Mn^{t}P1**]$^{+1}$. Upon reduction, however, the Mn α-spin in the quartet [**Mn^{t}P3**]^0 species becomes 3.27 (compared with 3.14 for [**Mn^{t}P1**]^0). The use of an aromatic linker, therefore, leads to a somewhat larger spill-over spin polarisation. This is presumably due to the delocalisation and/or electron-withdrawing effect of the bridging phenyl ring, which can be expected to facilitate the accommodation of an excess electron.

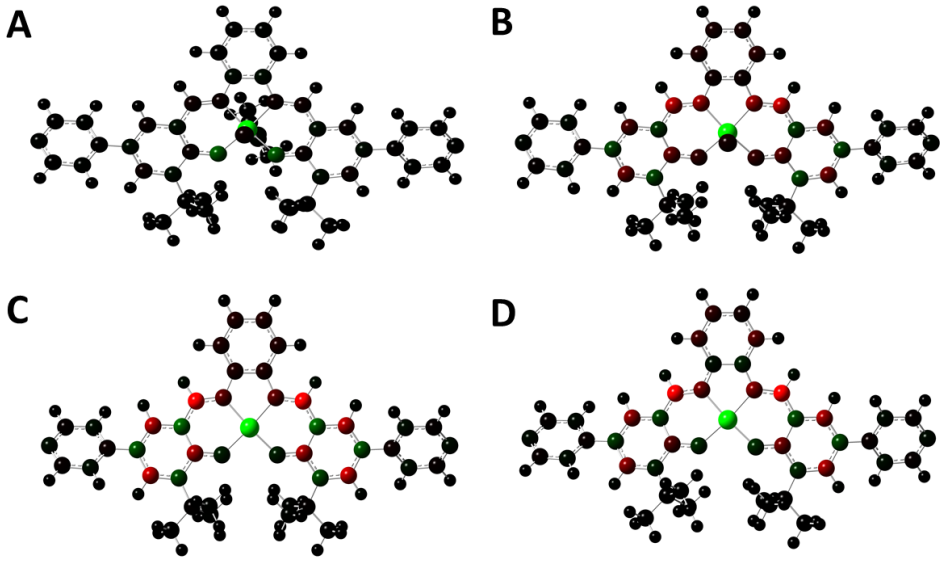

Figure 7. Colour representation of spin distribution with a range of –0.25 to +0.25 in **A** [**Mn^{t}P3Cl.DMF**]^0, **B** [**Mn^{t}P3Cl**]$^{-1}$, **C** [**Mn^{t}P3**]$^{-1}$, and **D** [**Mn^{t}P3**]$^{-2}$. Green represents excessive α-spins (up to 5), red represents (to different magnitudes) β-spins (up to –0.5), and black represents close to neutral states.

NBO analysis on the second reduction process (i.e. II_R – [**Mn^{t}P3**]$^{-1}$) shows a build-up of excess β-spins in [**Mn^{t}P3**]$^{-1}$ upon reduction from **[Mn^{t}P3]**^{0} (Figure 7), which is consistent with experimental observations. Closer inspection of the α- and β-spin values reveals a spill-over to the Mn centre, such that its excess α-spin is changed from 3.27 to 3.47. In comparison, for the alkyl analogues [**Mn^{t}P1**]^0 and [**Mn^{t}P1**]$^{-1}$, the Mn α-spin values change little from 3.14 for the former to 3.36 for the latter. This yet again demonstrates that the aromatic linker maintains a channel for communication that seemed less prominent for the alkyl analogue.

For the [**Mn^{t}P3**]$^{-1}$ to [**Mn^{t}P3**]$^{-2}$ reduction, i.e., III_R, the almost identical pictures shown in Figure 7C and D suggest that the nature of the species do not change substantially. For this process, the Mn excess α-spin goes from 3.47 to 1.00 (doublet) and 4.11 (quartet), which are quite different from those for **[Mn^{t}P3]**$^{-2}$. It also implies that the additional electron is shared by both the Mn centre as well as the ligand, and that the spin is distributed quite evenly between the two sides. This in part accounts for the subtle spectroscopic changes observed experimentally (Figure 6D). At this point, we again highlight the subtle differences in the nature of redox processes for a complex with an alkyl-linked (Figure 4) versus an aryl-linked (Figure 7) ligand, and that the reduction becomes increasingly ligand-based, for both **Mn^{t}P1** and **Mn^{t}P3**.

Electrochemical behaviour in the presence of CO_2

Solution state CV experiments were performed for all salen complexes in the presence of CO_2. A solution of analyte (1–2 mM) and proton source (2,2,2-trifluoroethanol [TFE]) in 0.1 M [(n-C_4H_9)$_4$N]PF_6/DMF was purged with CO_2 until gas saturation was reached (*ca* 0.28 M in MeCN and 0.23 M in DMF).[55] Representative aliphatic (**Mn^{t}P1Cl**) and aromatic (**Mn^{t}P3Cl**) complexes are profiled in depth.

Mn^{t}P1Cl did not show any significant electrochemical activity in the presence of CO_2 (Figure 8A); however, a number of gaseous and solution phase products were observed under a CO_2 atmosphere. There was no shift outside of experimental error in the I_R redox process (corresponding to the Mn(III/II) redox process).

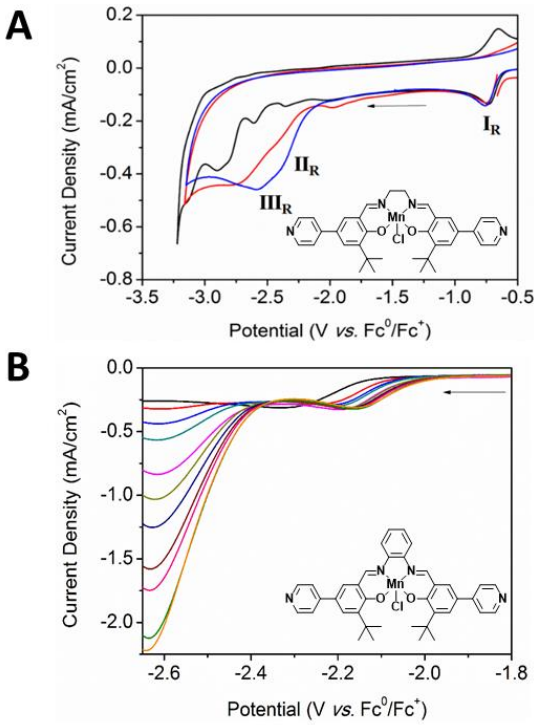

Figure 8. Solution state CVs showing the electrochemical response of **A Mn^{t}P1Cl** (1 mM) under saturation conditions of N_2 (black), CO_2 (red) and CO_2 with TFE (8 mmol) as a proton source (blue) and **B** under saturation of N_2 (black), CO_2 (red) and CO_2 with TFE (0.7 mmol-light blue, 1.4 mmol-green, 2.1 mmol-light pink, 2.8 mmol-yellow, 3.5 mmol-dark blue, 4.2 mmol-brown, 4.9 mmol-dark pink, 5.6 mmol-green and 6.3 mmol-orange). Return sweeps are not shown for clarity (0.1 M $[(n\text{-}C_4H_9)_4N]PF_6$/DMF as the supporting electrolyte, scan rate: 0.1 V s^{-1}, Fc (1 mM) was used as an internal standard).

Electrolysis of a bulk solution of **Mn^{t}P1Cl** complex (1.12 mM) resulted in the generation of CO and formic acid, as measured from the first 1.25 turnovers of the analyte after the passing of 1.2 C. Over 210 min, the production of both H_2 and CO began to plateau, indicating that the salen metal complex was reaching the end of its lifetime. The analyte also sustained current densities of approximately 0.24 mA/cm^2 during the experiment, with evidence of the density declining towards the end of the measurement. The bulk electrolysis solution was also analysed for additional liquid phase products *via* solution state ^{1}H NMR experiments, which revealed a peak at δ = 8.00 ppm corresponding to the generation of formic acid. Upon time-course measurements, this peak continued to grow (Figure S18, Supporting Information). A blank bulk electrolysis experiment in the absence of both CO_2 and **Mn^{t}P1Cl** was undertaken, demonstrating that no formic acid peaks were observed.

The aromatic Mn(III) salen metal complexes demonstrated improved electrochemical behaviour over the aliphatic systems. **Mn^{t}P3Cl** showed favourable reduction activity in the presence of CO_2 (Figure 8B). Only small

changes in the position of the I_R redox feature were observed. For the II_R ligand-based process, the peak increased and shifted anodically under CO_2 compared to under N_2 saturation. The anodic shift became greater with increasing concentrations of TFE, indicating CO_2 association. The III_R ligand reduction of **Mn^{t}P3Cl** only becomes significant upon the addition of TFE and indicates that a proton source is necessary for improved electrochemical activity. The absence of a current increase in this particular peak under N_2 with the Brønsted acid indicated that the process is not solely related to proton reduction to form H_2, but is more likely due to the reduction of CO_2. The reversibility of the first processes means that it is possible to calculate meaningful kinetics data for the interaction of the salen complex with CO_2 from reversible reactions (Equations 1-4, Supporting Information). An average K_{CO2} of 22.9 ± 5.3 M^{-1} was calculated for **Mn^{t}P3Cl** (Figure 8B). This value decreased upon the addition of electron donating groups to the backbone (Figure S16, Supporting Information). Finally, a chemical reduction was performed to validate the electrochemical observations (Figure S23, Supporting Information).

A bulk electrolysis experiment was performed on **Mn^{t}P3Cl** (1.15 mM) in 0.1 M [(*n*-$C_4H_9)_4N]PF_6$/DMF/MeCN (8:2) with TFE (0.63 M) at E_{pc} = –2.25 V *vs*. Fc^0/Fc^+, which was the limit of the solvent window (Figure S24, Supporting Information). As a result, the full III_R redox feature at E_{pc} = –2.64 V *vs*. Fc^0/Fc^+ could not be accessed. Applying a potential anodic of the III_R feature but cathodic of the II_R process resulted in CO and H_2 formation, as measured from the first 4.19 turnovers of the analyte over 3 h. Throughout the experiment, a linear relationship in the production of CO was maintained, indicating that the lifetime of the active species may be longer. The plateau in H_2 production cannot be attributed to the depletion of the proton source; if it were, there would be a corresponding decrease in CO production from the process, since the proton source is necessary to enhance the electrochemical activity. If the reduction could be shifted to a more accessible reduction potential, it may be possible to convert CO_2 at a faster rate. Over the course of the bulk electrolysis experiment on **Mn^{t}P3Cl**, the analyte sustained current densities of 0.29 mA/cm^2 with evidence of declining current density towards the end of the experiment. The Faradaic Efficiency for the conversion of CO_2 into CO was measured for all complexes (Table S2, Supporting Information).

CONCLUSIONS

This work has investigated the design and synthesis of a series of Mn(III) pyridyl salen-based metal complexes to examine their electrochemical behaviour under an inert atmosphere and in the presence of CO_2. Eight salen metal complexes incorporating both aliphatic and aromatic bridging moieties were synthesised in good yields and the variation in the salen backbone was explored to understand the factors that modulate the redox behaviour. Comprehensive characterisation was conducted using CV, IR and UV-Vis-NIR SEC experiments in tandem with DFT computations to examine the electrochemical properties of the complexes and the mechanism of reduction. Differences in the SEC experiments indicated that the aromatic bridging moiety facilitates electron delocalisation and a more stable radical upon reduction, since the aliphatic bridging moiety appears to inhibit electronic communication across the backbone. Finally, kinetic and electrochemical studies were performed where possible on the complexes in the presence of CO_2, revealing the generation of small quantities of CO and formic acid in trace amounts. The

intrinsically high reduction potentials that these complexes require precluded analysis of the electrochemical processes responsible for conversion, since they were limited by the available solvent windows and the solubilities of the salen metal complexes.

Two important conclusions can be drawn from the study of these complexes. Firstly, the backbone of the salen complex plays a vital role in its overall stability. The incorporation of the aromatic bridging diamine and the *tert*-butyl functional groups (i.e. **Mn^{t}P3Cl** and **Mn^{t}P4Cl**) are the most favourable for complex stability. The aromatic bridging moiety is superior to an aliphatic one, since the aromatic group facilitates electronic communication across the entire ligand. This said, the presence of electron donating groups reduces the stability of the complex as extra potential is required to access reduction processes. Modulating the functional groups on the aromatic bridging moiety tunes the potential of the reduction processes, which has previously been observed in work on one-electron oxidised species by Ottenwaelder and coworkers,[56] Shimazaki and coworkers,[57, 58] and Storr and co-workers.[59, 60] The *tert*-butyl functional group provides electrochemical stability to the salen backbone as it is reduced. Although some of the salen metal complexes were unstable upon reduction, a number of the aromatic, *tert*-butyl stabilised complexes demonstrated the potential to be electrochemically active in the presence of CO_2 and efforts are underway to stabilise their backbones for CO_2 reduction.

ASSOCIATED CONTENT

Supporting Information

Supporting information contains additional synthetic details, electrochemical and spectroelectrochemical data, and kinetics analyses. This material is available free of charge via the Internet at http://pubs.acs.org.

AUTHOR INFORMATION

Corresponding Authors

School of Chemistry, The University of Sydney, New South Wales, Australia 2006, Email: deanna.dalessandro@sydney.edu.au; kate.jolliffe@sydney.edu.au

Author Contributions

M.B.S. undertook all experimental components and B.C. undertook all computational modelling described in this manuscript. The computational sections of the manuscript was written by B.C., The remaining sections of the manuscript were written by M.B.S., with input from all authors. All authors have given approval to the final version of the manuscript.

Funding Sources

Australian Research Council; Science and Industry Research Fund; Japan Society for the Promotion of Science; National Science Foundation.

Notes

The authors declare no competing financial interests.

ACKNOWLEDGEMENTS

This work was supported by the Australian Research Council and the Science and Industry Endowment Fund (SIEF) as part of the 'Solving the Energy Waste Roadblock' venture, and Japan Society for the Promotion of Science. We gratefully acknowledge Dr Danielle Kennedy at the Commonwealth Scientific and Industrial Research Organisation (CSIRO) for her support in the provision of an OCE PhD top-up scholarship for M.B.S. We are also grateful to Dr Charles Machan from The University of Virginia and Dr Mark Reineke from The University of California, San Diego for their assistance with IR SEC and bulk electrolysis measurements, Dr Carol Hua for guidance on UV-Vis-NIR SEC, and provision of computational resources from RIKEN Advanced Center for Computing and Communication and from Institute of Molecular Science. C.P.K gratefully acknowledges NSF (CHE-1145893) for support.

REFERENCES

1. K. C. Gupta and A. K. Sutar, *Coord. Chem. Rev.*, 2008, **252**, 1420-1450.
2. P. Pfeiffer, E. Breith, E. Lübbe and T. Tsumaki, *Liebigs. Ann. Chem.*, 1933, **503**, 84-130.
3. D. J. Darensbourg, in *Synthetic Biodegradable Polymers*, eds. B. Rieger, A. Künkel, W. G. Coates, R. Reichardt, E. Dinjus and A. T. Zevaco, Springer Berlin Heidelberg, Berlin, Heidelberg, 2012, DOI: 10.1007/12_2011_135, pp. 1-27.
4. H. Khoshro, H. R. Zare, A. Gorji, M. Namazian, A. A. Jafari and R. Vafazadeh, *J. Electroanal. Chem.*, 2014, **732**, 117-121.
5. T. Kurahashi and H. Fujii, *J. Am. Chem. Soc.*, 2011, **133**, 8307-8316.
6. T. P. Yoon and E. N. Jacobsen, *Science*, 2003, **299**, 1691-1693.
7. S. V. Bhosale, C. H. Jani and S. J. Langford, *Chem. Soc. Rev.*, 2008, **37**, 331-342.
8. P. M. Usov, C. Fabian and D. M. D'Alessandro, *Chem. Commun.*, 2012, **48**, 3945-3947.
9. C. F. Leong, B. Chan, T. B. Faust, P. Turner and D. M. D'Alessandro, *Inorg. Chem.*, 2013, **52**, 14246-14252.
10. D. M. D'Alessandro, *Chem. Commun.*, 2016, **52**, 8957-8971.
11. D. M. D'Alessandro, J. R. R. Kanga and J. S. Caddy, *Aust. J. Chem.*, 2011, **64**, 718-722.
12. C. F. Leong, P. M. Usov and D. M. D'Alessandro, *MRS Bulletin*, 2016, **41**, 858-864.
13. M. B. Solomon, T. L. Church and D. M. D'Alessandro, *CrystEngComm*, 2017, **19**, 4049-4065.
14. A. Mahmood, W. Guo, H. Tabassum and R. Zou, *Adv. Energy Mat.*, 2016, **6**, 1600423-n/a.
15. J. Andrez, V. Guidal, R. Scopelliti, J. Pécaut, S. Gambarelli and M. Mazzanti, *J. Am. Chem. Soc.*, 2017, **139**, 8628-8638.
16. S. R. Borhade and S. B. Waghmode, *Tetrahedron Lett.*, 2008, **49**, 3423-3429.
17. L. Canali and D. C. Sherrington, *Chem. Soc. Rev.*, 1999, **28**, 85-93.
18. D. J. Darensbourg and J. C. Yarbrough, *J. Am. Chem. Soc.*, 2002, **124**, 6335-6342.
19. Z. Dong, X. Liu, J. Feng, M. Wang, L. Lin and X. Feng, *Eur. J. Org. Chem.*, 2011, **2011**, 137-142.
20. T. Linker, *Angew. Chem. Int. Ed.*, 1997, **36**, 2060-2062.
21. Y.-s. Liu, N.-n. Gu, P. Liu, X.-w. Ma, Y. Liu, J.-w. Xie and B. Dai, *Tetrahedron*, 2015, **71**, 7985-7989.
22. S. Qian-Ping, S. Zhi-Hao, L. Nian-Guang, T. Yu-Ping, L. Wei, T. Hao, Z. Wei, S. Min-Zhe and D. Jin-Ao, *Curr. Org. Chem.*, 2013, **17**, 2936-2970.
23. F. Trentin, A. Scarso and G. Strukul, *Tetrahedron Lett.*, 2011, **52**, 6978-6981.
24. M. B. Solomon, A. Rawal, James M. Hook, S. M. Cohen, C. P. Kubiak, K. A. Jolliffe and D. M. D'Alessandro, *RSC Adv.*, 2018, **8**, 24128-24142.
25. M. Holbach and M. Weck, *J. Org. Chem.*, 2006, **71**, 1825-1836.
26. R. Ji, K. Yu, L.-L. Lou and S. Liu, *J. Mol. Catal. A: Chem.*, 2013, **378**, 7-16.
27. F. Jutz, J.-D. Grunwaldt and A. Baiker, *J. Mol. Catal. A: Chem.*, 2008, **279**, 94-103.
28. G. Kowalski, J. Pielichowski and M. Jasieniak, *Appl. Catal., A*, 2003, **247**, 295-302.
29. V. Mirkhani, M. Moghadam, S. Tangestaninejad, I. Mohammadpoor-Baltork and N. Rasouli, *Catalysis Communications*, 2008, **9**, 219-223.
30. L. P. C. Nielsen, C. P. Stevenson, D. G. Blackmond and E. N. Jacobsen, *J. Am. Chem. Soc.*, 2004, **126**, 1360-1362.
31. M. North, P. Villuendas and C. Young, *Chem. Eur. J.*, 2009, **15**, 11454-11457.
32. G. A. E. Oxford, D. Dubbeldam, L. J. Broadbelt and R. Q. Snurr, *J. Mol. Catal. A: Chem.*, 2011, **334**, 89-97.
33. P. J. Pospisil, D. H. Carsten and E. N. Jacobsen, *Chem. Eur. J.*, 1996, **2**, 974-980.
34. X. Zheng, C. W. Jones and M. Weck, *J. Am. Chem. Soc.*, 2007, **129**, 1105-1112.
35. J. Desilvestro and S. Pons, *J. Electroanal. Chem. Interfacial Electrochem.*, 1989, **267**, 207-220.
36. J. Hawecker, J.-M. Lehn and R. Ziessel, *J. Chem. Soc., Chem. Commun.*, 1984, DOI: 10.1039/C39840000328, 328-330.
37. S. Berger, A. Klein, W. Kaim and J. Fiedler, *Inorg. Chem.*, 1998, **37**, 5664-5671.
38. O. Ishitani, M. W. George, T. Ibusuki, F. P. A. Johnson, K. Koike, K. Nozaki, C. Pac, J. J. Turner and J. R. Westwell, *Inorg. Chem.*, 1994, **33**, 4712-4717.
39. D. R. Coulson, L. C. Satek and S. O. Grim, in *Inorg. Synth.*, John Wiley & Sons, Inc., 2007, DOI: 10.1002/9780470132449.ch23, pp. 121-124.
40. I. S. Zavarine and C. P. Kubiak, *J. Electroanal. Chem.*, 2001, **495**, 106-109.

41. M. J. Frisch, G. W. Trucks, H. B. Schlegel, G. E. Scuseria, M. A. Robb, J. R. Cheeseman, G. Scalmani, V. Barone, B. Mennucci, G. A. Petersson, H. Nakatsuji, M. Caricato, X. Li, H. P. Hratchian, A. F. Izmaylov, J. Bloino, G. Zheng, J. L. Sonnenberg, M. Hada, M. Ehara, K. Toyota, R. Fukuda, J. Hasegawa, M. Ishida, T. Nakajima, Y. Honda, O. Kitao, H. Nakai, T. Vreven, J. A. Montgomery, J. E. Peralta, F. Ogliaro, M. Bearpark, J. J. Heyd, E. Brothers, K. N. Kudin, V. N. Staroverov, R. Kobayashi, J. Normand, K. Raghavachari, A. Rendell, J. C. Burant, S. S. Iyengar, J. Tomasi, M. Cossi, N. Rega, J. M. Millam, M. Klene, J. E. Knox, J. B. Cross, V. Bakken, C. Adamo, J. Jaramillo, R. Gomperts, R. E. Stratmann, O. Yazyev, A. J. Austin, R. Cammi, C. Pomelli, J. W. Ochterski, R. L. Martin, K. Morokuma, V. G. Zakrzewski, G. A. Voth, P. Salvador, J. J. Dannenberg, S. Dapprich, A. D. Daniels, Farkas, J. B. Foresman, J. V. Ortiz, J. Cioslowski and D. J. Fox, *Journal*, 2016, DOI: citeulike-article-id:9096580.
42. J. P. Perdew, *Electronic Structures of Solids*, Akademie Berlin, Berlin, 1991.
43. A. D. Becke, *J. Chem. Phys.*, 1993, **98**, 5648-5652.
44. A. E. Reed, L. A. Curtiss and F. Weinhold, *Chem. Rev.*, 1988, **88**, 899-926.
45. N. Mardirossian and M. Head-Gordon, *Mol. Phys.*, 2017, **115**, 2315-2372.
46. J. J. Determan, K. Poole, G. Scalmani, M. J. Frisch, B. G. Janesko and A. K. Wilson, *J. Chem. Theory Comput.*, 2017, **13**, 4907-4913.
47. A. V. Marenich, C. J. Cramer and D. G. Truhlar, *J. Phys. Chem. B*, 2009, **113**, 6378-6396.
48. C. T. Lyons and T. D. P. Stack, *Coord. Chem. Rev.*, 2013, **257**, 528-540.
49. R. M. Clarke and T. Storr, *Dalton Trans.*, 2014, **43**, 9380-9391.
50. Y. Zidane, A. Ourari, T. Bataille, P. Hapiot and D. Hauchard, *J. Electroanal. Chem.*, 2010, **641**, 64-70.
51. Y.-P. Ou, J. Zhang, M. Xu, J. Xia, F. Hartl, J. Yin, G.-A. Yu and S. H. Liu, *Chem. Asian J.*, 2014, **9**, 1152-1160.
52. M. Nagata, Y. Futami, N. Akai, S. Kudoh and M. Nakata, *Chem. Phys. Lett.*, 2004, **392**, 259-264.
53. A. Korte, A. Mardyukov and W. Sander, *Aust. J. Chem.*, 2014, **67**, 1324-1329.
54. E. E. Shehata, M. S. Masoud, E. A. Khalil and A. M. Abdel-Gaber, *J. Mol. Liq.*, 2014, **194**, 149-158.
55. A. Gennaro, A. A. Isse and E. Vianello, *J. Electroanal. Chem. Interfacial Electrochem.*, 1990, **289**, 203-215.
56. D. de Bellefeuille, M. S. Askari, B. Lassalle-Kaiser, Y. Journaux, A. Aukauloo, M. Orio, F. Thomas and X. Ottenwaelder, *Inorg. Chem.*, 2012, **51**, 12796-12804.
57. Y. Shimazaki, T. D. P. Stack and T. Storr, *Inorg. Chem.*, 2009, **48**, 8383-8392.
58. H. Oshita, T. Yoshimura, S. Mori, F. Tani, Y. Shimazaki and O. Yamauchi, *JBIC Journal of Biological Inorganic Chemistry*, 2018, **23**, 51-59.
59. T. J. Dunn, C. F. Ramogida, C. Simmonds, A. Paterson, E. W. Y. Wong, L. Chiang, Y. Shimazaki and T. Storr, *Inorg. Chem.*, 2011, **50**, 6746-6755.
60. M. Kawai, T. Yamaguchi, S. Masaoka, F. Tani, T. Kohzuma, L. Chiang, T. Storr, K. Mieda, T. Ogura, R. K. Szilagyi and Y. Shimazaki, *Inorg. Chem.*, 2014, **53**, 10195-10202.

A series of discrete, functionalised Mn(III) pyridyl salen metal complexes with varying aliphatic and aromatic bridging diamines have been evaluated and their spectroelectrochemical properties probed.

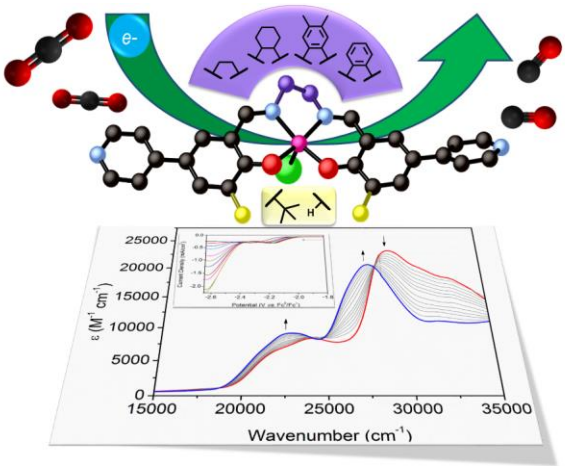

For Table of Contents Only